2021

Simulations of Single- and Two-Tone Tm-doped Optical Fiber Laser Amplifiers

Tathagata Goswami
Portland State University, tgoswami@pdx.edu

J. Grosek
Air Force Research Laboratory

Jay Gopalakrishnan
Portland State University, gjay@pdx.edu

Citation Details

Goswami, T., Grosek, J., & Gopalakrishnan, J. (2021). Simulations of single-and two-tone Tm-doped optical fiber laser amplifiers. Optics Express, 29(8), 12599-12615.

Research Article | Vol. 29, No. 8 / 12 April 2021 / Optics Express 12599
Optics EXPRESS

Simulations of single- and two-tone Tm-doped optical fiber laser amplifiers

T. GOSWAMI,[1] J. GROSEK,[2,*] AND J. GOPALAKRISHNAN[1]

[1]Portland State University, PO Box 751, Portland, OR 97207, USA
[2]Air Force Research Laboratory, 3550 Aberdeen Ave SE, Albuquerque, NM 87117, USA
[*]Jacob.Grosek.1@us.af.mil

Abstract: This work uses numerical simulations of a thulium-doped optical fiber amplifier to predict various performance characteristics such as peak temperatures, expected output powers and efficiencies, presence of amplified spontaneous emission (ASE), and transverse mode instability (TMI) onset power thresholds. Single- and two-tone configurations are studied. In the latter case, the two laser sources are separated in frequency by the amount that corresponds to the peak Raman gain, and a few seed ratios at various total seed powers are examined. The goal is to provide the field with pertinent information on what is feasible for this type of amplifier.

1. Introduction

Typical high-power beam combinable active gain fiber amplifiers are seeded with only one laser source, usually referred to as the *signal* light. This configuration will be denoted as a *single-tone* amplifier. However, when more than one highly coherent laser source is seeded into the amplifier, a laser gain competition (LGC) between the various laser wavelengths ensues within the active dopant, and this may be advantageous for power scaling purposes [1]. Dajani et al. [2,3] were able to utilize the LGC configuration, building upon an idea by Weßels et al. [4], in order to demonstrate the suppression of the stimulated Brillouin scattering (SBS) nonlinearity in optical fibers. In their studies, an Yb-doped amplifier was seeded with two lasers, and then by carefully selecting the ratio of seed powers (a.k.a. the *seed ratio*) and by separating the wavelengths of the two lasers by at least $\Delta\lambda \sim >10$ nm, a substantial SBS mitigation was achieved. They called this a *two-tone* amplifier configuration. The additional laser source for the two-tone configuration usually has a core-pumped laser source that is in-between the wavelength of the pump light and the signal light; hereafter, this wavelength shall be referred to as the *tone*; thus, $\lambda_p < \lambda_t < \lambda_s$.

Generally, optical nonlinearities, i.e. SBS, stimulated Raman scattering (SRS), Kerr effects, four-wave mixing (FWM), etc., arise in high-power fibers because of long interaction lengths, allowing for the nonlinear processes to build-up, and/or because of high irradiance levels of the propagating light, allowing for a more pronounced interaction with the medium and/or with the optical field itself. The two-tone configuration helps suppress the onset of optical nonlinearities by reducing the effective length over which any laser field has a high power (thus, high irradiance). In many cases, a two-tone amplifier can be tuned to produce about the same output signal power, with a similar amplifier efficiency, as a comparable single-tone amplifier. The two-tone configuration has at least two other benefits as well, including the fact that heat generation is further spread out along the fiber length, leading to the lower peak temperatures [5], and this configuration has been shown to mitigate the onset of amplified spontaneous emission (ASE), and therefore also parasitic lasing [6].

The difficulty of lasing and/or amplifying a laser signal in the 2.1-2.2 μm regime is due to the fact that the gain spectrum of the thulium (Tm) dopant rapidly diminishes beyond 2.1 μm, as can be ascertained from Fig. 1. Part of this challenge is that it will be difficult to create a strong seed power for the signal, and combined with the low gain in this wavelength range, one expects to observe significant amounts of amplified spontaneous emission (ASE), and possibly parasitic

#418095 https://doi.org/10.1364/OE.418095
Journal © 2021 Received 21 Dec 2020; revised 1 Apr 2021; accepted 1 Apr 2021; published 9 Apr 2021

Optics EXPRESS

lasing [6]. However, above 2100 nm in wavelength there are some propitious atmospheric transmission windows, where one can expect to get up to about 95% transmission, as seen in Fig. 2 [7–9].

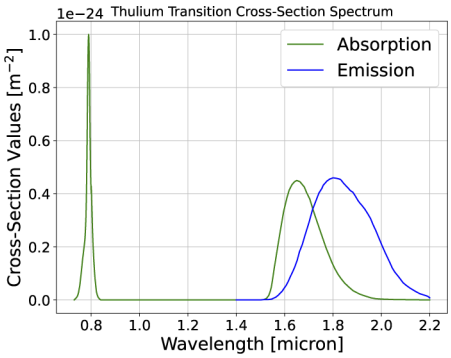

Fig. 1. Absorption and emission cross-section spectra of the thulium dopant [10].

Tm-doped amplifiers can have higher dopant concentrations than ytterbium-doped amplifiers, and thus they are more susceptible to cross-relaxations and upconversions (see Fig. 3) [11]. The strong cross-relaxation in the thulium kinetics model can almost double the optical-to-optical (O-O) efficiency of the amplifier. Nonetheless heat generation in the fiber is still a significant issue that can either degrade($\sim$ >85°C), or even destroy ($\sim$ >125°C), the polymer coating. The trade-off to be considered is that the heat deposition per unit length will decrease as the dopant concentration is lowered; however, the cross-relaxation process also diminishes in direct proportion to the dopant concentration. Without a pronounced cross-relaxation, the fiber efficiency (η) will tend towards what would be expected from the quantum defect: $\eta \sim 1 - \lambda_p/\lambda_s$, which would vastly increase the amount of energy being deposited as heat per unit length. This study will use the steady-state thulium energy level kinetics model presented in McComb's dissertation [12], and will only consider the typical co-/cladding-pumped configuration, where the wavelength of the pump light is near the peak absorption around 790-793 nm. In the absorption/emission dataset that we have [10], this peak occurs at 790 nm.

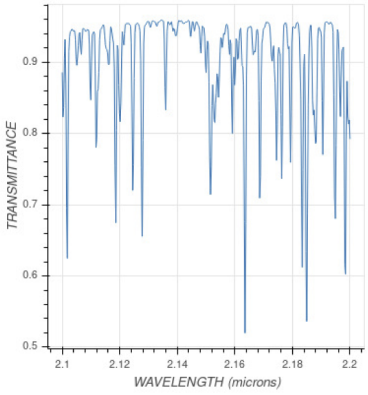

Fig. 2. Atmospheric transmittance in the wavelength range 2.1-2.2 μm.

The main goal of this paper is to present relevant information, extracted from computer simulation results, on the practicality and feasibility of a Tm-doped fiber amplifier operating in the 2100-2200 nm wavelength regime. Our detailed numerical simulations will investigate

Optics EXPRESS

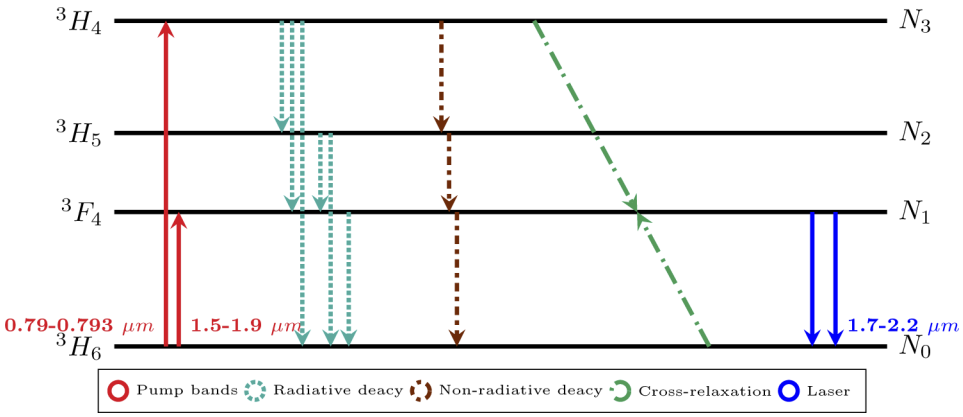

Fig. 3. Simplified thulium electron energy level diagram.

different dopant concentrations, single- and two-tone amplifier configurations, various seed ratios and total seed powers in a straight fiber, or one that is circularly bent (R_{bend} = 80 mm), all at three specific signal wavelengths: 2110 nm, 2133 nm, and 2170 nm. For the two-tone configured fibers, the tone wavelength is chosen to be exactly 13.2 THz higher in frequency than the signal wavelength in order to take advantage of the peak Raman gain in a fused silica medium (see Fig. 4). This makes for a hybrid gain amplifier, including the active Tm dopant [13] and gain from the SRS optical nonlinearity [14], with the hope of, at least slightly, improving the suppression of the ASE and reducing the amplifier length that achieves 95% pump absorption. Note that for the two-tone configured amplifier, in order to better spread the heat deposition more evenly along the fiber, one would ideally want the tone wavelength to be close to the average of the pump

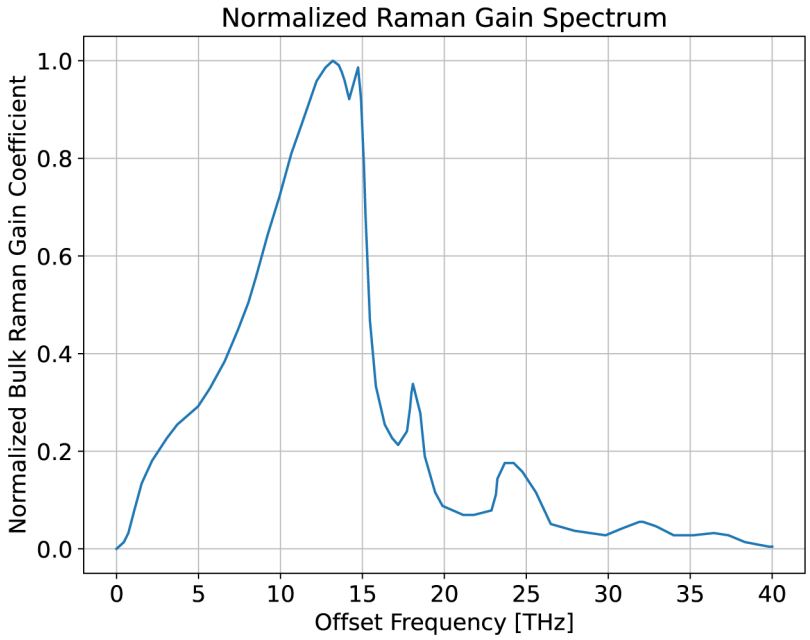

Fig. 4. Experimentally measured normalized bulk Raman gain coefficient as the offset frequency between the Raman pump and Stokes waves varies [12].

Optics EXPRESS

and signal wavelengths: $\lambda_t \sim (\lambda_p + \lambda_s)/2$. Since this is not the case for our Tm-doped amplifier, there likely will not be significant difference between the single- and two-tone longitudinal heat profiles. We will present expected peak temperatures within the fiber, signal output powers, and signal amplification efficiencies, all while allowing ASE to arise naturally in the amplifier based on the given conditions. Moreover, we will show the effect of wavelength on the mode-bend-loss values in the presence of three distinct steady-state thermal profiles. At the 2110 nm signal wavelength, various transverse mode instability (TMI) power thresholds are predicted in a straight fiber (compare with numerical TMI study in Tm-doped amplifier by Smith and Smith [15]).

The paper is organized as follows. In section 2, we describe the computational model for this problem, including how both light propagation and thermal issues are handled in the simulation. Section 3 presents the modeling results, starting with the wavelength and temperature dependence of the guided core mode-bend-losses near 2 μm (subsection 3.1) and a brief comparison between single- and two-tone amplifier output signal powers (subsection 3.2). Then, subsection 3.3 provides results regarding the effects of varying the total dopant concentration. The onset of ASE in the amplifier is studied in subsection 3.4 as seeding conditions are altered. Finally, we explore the onset power thresholds of the TMI for an amplifier with a signal wavelength of 2.11 μm, delineated in subsection 3.5. Each of these result subsections quantify aspects of complicated trade-space that pertains to Tm-doped amplifiers operating in the 2.1-2.2 μm wavelength range.

2. Model description

This model considers a continuous-wave, weakly guided, step-index Tm-doped optical fiber amplifier with core radius $r_{core} = 10\,\mu$m, surrounded by a pure fused silica inner cladding that extends to radius $r_{clad} = 200\,\mu$m, and a polymer jacket of thickness 75 μm ($r_{fiber} = 275\,\mu$m). The refractive index of the core and the inner cladding regions are denoted as n_{core} and n_{clad}, respectively. The core numerical aperture $\left(NA_{core} = ({n_{core}}^2 - {n_{clad}}^2)^{1/2}\right)$ is 0.09. Generally, our model follows the same coupled mode theory approach as described in Naderi et al. [16], though we use a slightly different notation. Other notable differences include the fact that we modify the governing equations for the inclusion of the ASE wavelengths, the intrinsic loss of the glass, the loss due to OH^{-1} (hydroxide) contamination, and the mode-bend-loss (when the fiber is coiled). Moreover, the transverse domain is discretized using higher (polynomial) order finite elements, such that the elements conform to the fiber boundaries. All integrations over the transverse domain are computed using at least third-order Lagrangian element spaces ensuring higher precision calculations [17].

Only the transverse guided core modes are included in the model for the tone, signal, and ASE wavelengths, and the pump light is modeled as a planewave [13,18]. The mode profiles and pump planewave extend throughout the core and inner cladding regions, but are considered to be negligibly small in the polymer coating region. The total number of fiber core modes is given by M_ℓ, where ℓ indexes the given wavelength. Each mode is comprised of an amplitude Y^ℓ, a transverse profile φ^ℓ, and a corresponding propagation constant β^ℓ. We compute the mode data by solving the eigenvalue problem,

$$\left(\Delta_{xy} + k_\ell^2 n^2\right)\varphi_m^\ell = \left(\beta_m^\ell\right)^2 \varphi_m^\ell, \qquad m = 1, \ldots, M_\ell\,. \tag{1}$$

Under the fiber coiling situations, the corresponding mode-loss values are calculated using the technique outlined by Schermer & Cole [19]. Our propagation model is currently not capable of handling coiled fiber mode profiles, so instead we use the straight fiber mode profiles. Though we do use the proper propagation constants and mode-bend-losses. Even still, after some numerical testing we found that in all cases pertinent to our investigations, comparing the coiled ($R_{bend} = 80$ mm) and straight fibers and including multiple wavelengths and thermal load conditions, the mode overlaps with the core (gain) region of the fibers only varies by 5.3% at most. This would

Optics EXPRESS

not hold true under tighter bends. Likely, the low variation in mode overlaps is due to the fact that Tm-doped fiber amplifiers have larger core numerical apertures (especially compared to Yb-doped amplifiers), which limit the mode deformation significantly. One consequence of this is that the gain saturation is maximized, which means that, in most situations, our results show best-case performance metrics.

This simulation only accounts for the forward propagating ASE, and only considers the fundamental mode at each ASE wavelength. Though it is certainly possible to include backward propagating light in the model, and backward ASE affects the onset of the TMI [20,21], this effort is only attempting to indicate when ASE will be an issue, not to accurately model its quantity nor its precise effects on amplifier performance. Moreover, including any backward propagating light would significantly increase the simulation runtime. We feel that this approach offers a fair indication of when ASE will become prominent in the amplifier, while keeping the simulations computationally tractable.

2.1. Governing equations

The model focuses on the situation where all of the light propagates only in the forward direction ($+z$) along the longitudinal length of the fiber. The effective index of refraction of the l^{th} mode at the given wavelength (ℓ) is represented by $n_l^\ell = \beta_l^\ell / k_\ell$, where the vacuum wavenumber is $k_\ell = \omega_\ell / c$. The steady-state active gain via stimulated emission is denoted as g_ℓ [m^{-1}], the steady-state active gain via spontaneous emission is represented with $\mathfrak{g}_\text{a}$ [m^{-1}], and the bulk Raman gain coefficient is given by g_R [m/W]. Although Raman gain occurs between the ASE wavelengths, and between the laser sources and ASE wavelengths, these interactions are neglected since the model is not attempting to accurately capture the conditions once there are significant amounts of ASE power present in the fiber. The dimensionless quantity for the Raman gain is $\Upsilon_\text{R}^{\ell=\text{t}} = -\omega_\text{t}/\omega_\text{s}$ for the tone, and $\Upsilon_\text{R}^{\ell=\text{s}} = 1$ for the signal. We use the complement wavelength index such that $\ell^c = \text{t}$ when $\ell = \text{s}$, and $\ell^c = \text{s}$ when $\ell = \text{t}$. The quantity $\delta n = (dn/dT)\delta T$ represents the perturbation in the index of refraction of the fiber due to the heat generated inside the fiber. The value $\alpha_\text{loss}>0$ is the sum of the background silica-, hydroxide contamination-, and mode-bend-losses [m^{-1}]. The losses at the pump wavelength are considered to be insignificant. The fiber transverse cross-section that includes the core and inner cladding regions is represented by $\Omega_{z_0} = \left\{(x,y,z)|x^2+y^2 \le r_\text{clad}^2; z = z_0 \in [0,L]\right\}$. The wavelength bandwidth over which the spontaneous emission occurs, namely the bin bandwidth for the five central ASE wavelengths, is denoted as $\Delta\lambda_\text{ASE}$. Finally, I_ℓ denotes the irradiance of the light with a wavelength indexed by ℓ.

For the tone and signal wavelengths ($\ell \in \{\text{t},\text{s}\}$), where there are $M_{\ell\in\{\text{t,s}\}} = 3$ guided core modes (LP_{01} and both orientations of LP_{11}), and $l = 1,\ldots,M_\ell$, the propagation is governed by

$$\begin{aligned} \frac{dY_l^\ell}{dz} &= -\frac{\alpha_\text{loss}^\ell}{2} Y_l^\ell + \sum_{m=1}^{M_\ell} e^{i(\beta_m^\ell - \beta_l^\ell)z} K_{lm}^\ell Y_m^\ell \\ \text{where, } K_{lm}^\ell &= \int_{\Omega_z} \left(\frac{k_\ell}{2\beta_l^\ell} g_\ell + \frac{k_\ell \Upsilon_\text{R}^\ell g_\text{R} I_{\ell^c}}{2\beta_l^\ell} + \frac{ik_\ell^2}{2\beta_l^\ell}\delta n \right) n \varphi_m^\ell \overline{\varphi_l^\ell}\, dxdy\,. \end{aligned} \tag{2}$$

Optics EXPRESS

For the ASE wavelengths (ℓ = a), only the fundamental mode is modeled ($M_{\rm a}$ = 1 and $l = 1 = m$):

$$\begin{aligned} \frac{dY_1^{\rm a}}{dz} &= K_{11}^{\rm a} Y_1^{\rm a} - \frac{\alpha_{\rm loss}^{\rm a}}{2} Y_1^{\rm a} + C_{11}^{\rm a} \mathcal{Y}_1^{\rm a}, \\ \text{where, } K_{11}^{\rm a} &= \int_{\Omega_z} \left(\frac{k_{\rm a}}{2\beta_1^{\rm a}} g_{\rm a} + \frac{ik_{\rm a}^2}{2\beta_1^{\rm a}} \delta n \right) n \varphi_1^{\rm a} \overline{\varphi_1^{\rm a}}\, dxdy, \\ C_{11}^{\rm a} &= \int_{\Omega_z} \frac{k_{\rm a}}{2\beta_1^{\rm a}} \mathfrak{g}_{\rm a} n \varphi_1^{\rm a} \overline{\varphi_1^{\rm a}}\, dxdy, \quad \text{and} \quad \mathcal{Y}_1^{\rm a} = \sqrt{\frac{2\mu_0 \hbar c^3}{n_1^{\rm a} \lambda_{\rm a}^3} \Delta\lambda_{\rm ASE}}\,. \end{aligned} \tag{3}$$

For the (planewave) pump wavelength (ℓ = p), only the irradiance is modeled:

$$\frac{dI_{\rm p}}{dz} = \left[\left(\frac{r_{\rm core}}{r_{\rm clad}} \right)^2 \frac{1}{|\Omega_z^{\rm core}|} \int_{\Omega_z^{\rm core}} g_{\rm p}\, dxdy \right] I_{\rm p}\,. \tag{4}$$

where $\Omega_{z_0}^{\rm core} = \left\{ (x,y,z) | x^2 + y^2 \le r_{\rm core}^2; z = z_0 \in [0, L] \right\}$.

Next, we describe how the above quantities are coupled to the thermal evolution. The change in the fiber temperature compared to the ambient temperature (25°C), is a function of x, y, z, and t, and we denote it by $\delta T(x,y,z,t)$. It satisfies the heat equation with a source term (Q) representing the net absorption along the fiber, primarily due to the gain mechanisms. An analysis of the relative sizes of derivatives in the heat equation indicates that $\partial_z^2[\delta T]$ may be neglected. Doing so, we solve the following time dependent transverse heat Eq. (5) on the transverse domains $\Omega_{z_0}^{\rm fiber} = \left\{ (x,y,z) | x^2 + y^2 \le r_{\rm fiber}^2; z = z_0 \in [0, L] \right\}$ at each discrete longitudinal point along the fiber, with a zero Dirichlet boundary condition at the boundary $r = r_{\rm fiber}$ denoted by $\partial\Omega_{z_0}^{\rm fiber}$.

$$\begin{aligned} \frac{\partial[\delta T]}{\partial t} &= \alpha_{\rm therm}^{\rm SiO_2} \Delta_{xy}[\delta T] + \frac{\alpha_{\rm therm}^{\rm SiO_2}}{\kappa_{\rm therm}^{\rm SiO_2}} Q(I_{\rm s}, I_{\rm t}, I_{\rm p}, I_{\rm a}), \qquad (x,y) \in \Omega_{z_0}^{\rm fiber}, \quad t \in [0, t_{\rm final}], \\ \delta T(x,y,z_0,t) &= 0 \text{ for } (x,y) \in \partial\Omega_{z_0}^{\rm fiber} \quad \text{and} \quad \delta T(x,y,z_0,0) = 0\,, \end{aligned} \tag{5}$$

where $\alpha_{\rm therm}^{\rm SiO_2}$ and $\kappa_{\rm therm}^{\rm SiO_2}$ are the thermal diffusivity and conductivity of glass, respectively. Note that the temperature is incorporated into the prior propagation equations via the perturbation to the refractive index: $\delta n = (dn/dT)\delta T$, where dn/dT is a measured thermo-optic coefficient [°C^{-1}]. Although heat generated from the Raman gain process occurs over the entire cross-sectional overlap area between the relevant irradiance profiles, the vast majority of this heat is generated within the core region. Thus, we only consider heat generation in the core region:

$$Q \approx -\Big(\underbrace{g_{\rm s} I_{\rm s} + g_{\rm t} I_{\rm t} + g_{\rm p} I_{\rm p} + \sum_{m=1}^{M_{\rm a}} g_{{\rm a}_m} I_{{\rm a}_m}}_{\text{net active gain (stimulated emission)}} + \underbrace{\sum_{m=1}^{M_{\rm a}} \mathfrak{g}_{{\rm a}_m} I_{{\rm a}_m}}_{\text{net active gain (spontaneous emission)}} + \underbrace{\sum_{\ell \in \{\rm t,s\}} \Upsilon_{\rm R}^{\ell} g_{\rm R} I_{\rm s} I_{\rm t}}_{\text{net Raman gain}} - \underbrace{\sum_{\ell \in \{\rm t,s,a\}} \alpha_{\rm therm}^{\ell} I_{\ell}}_{\text{absorption losses}} \Big), \tag{6}$$

where the absorption losses ($\alpha_{\rm therm}^{\ell}$>0) sum the hydroxide contamination and background silica (via phonon absorption) losses. For simplicity and speed of calculations, this model uses the thermal parameters for glass in the polymer region. However, in order to improve the accuracy of the reported change in temperature in the fiber, we approximately correct the change in temperature value, as if all calculations were done with the proper polymer thermal parameters and appropriate boundary condition at the glass-polymer interface, by using the steady-state thermal profile that one would get if the heat generation occurred uniformly in the active gain

Optics EXPRESS

region (core region) of the fiber:

$$\delta T(r) = \frac{q_{\text{heat}}}{4\pi} \begin{cases} \frac{2}{\kappa_{\text{therm}}^{\text{SiO}_2}} \ln\left(\frac{r_{\text{clad}}}{r_{\text{core}}}\right) + \frac{2}{\kappa_{\text{therm}}^{\text{poly}}} \ln\left(\frac{r_{\text{fiber}}}{r_{\text{clad}}}\right) + \frac{1}{\kappa_{\text{therm}}^{\text{SiO}_2}} \left(1 - \left(\frac{r}{r_{\text{core}}}\right)^2\right), & r \in \left[0, r_{\text{core}}\right] \\ \frac{2}{\kappa_{\text{therm}}^{\text{SiO}_2}} \ln\left(\frac{r_{\text{clad}}}{r}\right) + \frac{2}{\kappa_{\text{therm}}^{\text{poly}}} \ln\left(\frac{r_{\text{fiber}}}{r_{\text{clad}}}\right), & r \in \left(r_{\text{core}}, r_{\text{clad}}\right] \\ \frac{2}{\kappa_{\text{therm}}^{\text{poly}}} \ln\left(\frac{r_{\text{fiber}}}{r}\right), & r \in \left(r_{\text{clad}}, r_{\text{fiber}}\right] \end{cases}, \quad (7)$$

where, as previously mentioned, r_{fiber} is the radius of the entire fiber, including the polymer. The thermal conductivity of the polymer is denoted as $\kappa_{\text{therm}}^{\text{poly}}$. In this case, the peak change in temperature always occurs at the center of the fiber cross-section, and is given by

$$\delta T_{\text{peak}} = \delta T(r = 0) = \frac{q_{\text{heat}}}{4\pi} \left[\frac{2}{\kappa_{\text{therm}}^{\text{SiO}_2}} \ln\left(\frac{r_{\text{clad}}}{r_{\text{core}}}\right) + \frac{2}{\kappa_{\text{therm}}^{\text{poly}}} \ln\left(\frac{r_{\text{fiber}}}{r_{\text{clad}}}\right) + \frac{1}{\kappa_{\text{therm}}^{\text{SiO}_2}} \right]. \quad (8)$$

This correction to the reported change in temperature value is derived by approximating the uniform heat deposition per unit length (q_{heat}) using the actual full heat generation in the amplifier simulation (Q), i.e.,

$$q_{\text{heat}}(z_0) \approx \iint_{\Omega_{z_0}^{\text{core}}} Q(x, y, z_0)\, d\Omega_z\,.$$

Then, using either relation (8) or relation (7), one can very reasonably approximate the peak change in temperature in the transverse cross-section of the fiber or find the approximate peak temperature in the polymer jacket of the fiber.

3. Numerical simulation results

All the simulations are done using a C++ code built atop the multi-physics finite element software library NGSolve [22,23]. In all of our runs, we have included experimentally calculated values for background silica loss and OH^{-1} contamination loss (1 ppm) extracted from [24, Fig. 2]. The thulium absorption/emission cross-section values are evaluated using the data extracted from [10]. Moreover, this model considers ASE within the 1.9-2.15 μm wavelength band by binning this region into five equally sized bins. The first bin has a central wavelength set at 1925 nm, and each bin spans $\Delta\lambda_{\text{ASE}} = 50$ nm in wavelength. Using more ASE bins over the same region is more accurate, since each bin references the gain parameters at the central wavelength, which vary over the ASE wavelength window. However, based on our numerical tests, so long as the ASE levels power remain low ($\sim$ <5 W), five bins produce results that are within a few percent of those found when twenty five bins are used. The total dopant concentration is uniformly distributed throughout the fiber core region, and is formulated as $N_{\text{total}} = \left(3 \cdot 10^{26}\right) \mathcal{N}_{\text{factor}}$ $\left[\text{ions/m}^3\right]$, where $\mathcal{N}_{\text{factor}}$ is a unitless scaling factor. Additionally, the fiber length is always set at the point where 95% of the pump power has been absorbed ($L \equiv L_{95\%}$). Seed ratios are always presented as the tone power to the signal power (P_{t}:P_{s}) in its reduced fraction form. Finally, in all cases when the amplifier is coiled, the bending is circular such that $R_{\text{bend}} = 80$ mm all along the fiber length.

3.1. Thermally dependent mode-bend-loss

When the amplifier is coiled, the calculation of the mode-bend-loss values account for thermal effects by altering the refractive index according to thermal profiles, utilizing relation (7), at specified discrete peak change in temperature values. Figure 5 shows the computed mode-bend-loss behavior at three different fiber peak change in temperatures, namely 0°C, 100°C, and 200°C, as the wavelength varies around 2 μm. In this plot, the mode-bend-losses increase with the wavelength for the guided core modes because longer laser wavelengths result in fiber

Optics EXPRESS

waveguides that are closer to being robustly single-mode. However, the thermal lensing effect reduces the mode-bend-loss values by increasing the numerical aperture of the fiber core region, and therefore its V-number. The kinks in this plot may be due to the fact that our mode solver is finding degenerate modes compared to what it found at other wavelengths. However, this is not evident in the numerical results, which are always finding only one solution for the fundamental mode, and for each orientation of the LP_{11} mode. For now these kinks may be considered part of the uncertainty in the calculated mode losses.

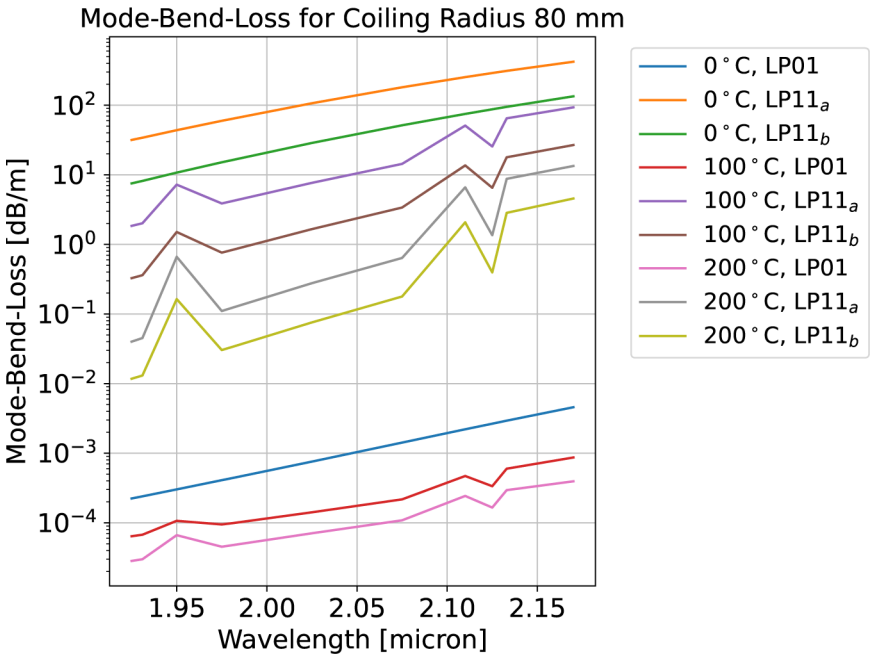

Fig. 5. Mode-bend-loss behavior under three different temperature profiles.

3.2. *Single- and two-tone output signal power comparisons*

In this brief study, we search for the two-tone seed ratios that either match the single-tone amplifier output signal power or maximize the amplifier output signal power in a cold amplifier. In all cases the fiber is coiled, its length is set at where 95% pump absorption occurs, and the amplifier is given 1 kW of launched pump power and has a total seed power, summing the tone and signal values across all modes, of 100 W. Heating effects are not considered. For λ_s = 2110 nm, the single- and two-tone configured amplifiers produce nearly identical signal output powers when the two-tone seed ratio is 21:10. However, the amplifier reaches its maximum output signal power when a 1:1 ratio is used in the two-tone configuration. For the signal wavelengths of 2133 nm and 2170 nm, the single-tone configuration seems to produce the maximum output signal power for the amplifier. For these wavelengths, we checked seed ratios as low as 1:50 for the two-tone configured amplifier, and the output signal powers were increasing as this seed ratio decreased. It is worth noting that lower seed ratios tend to be less beneficial for SBS mitigation.

3.3. *Effects of the dopant concentration*

In this investigation important amplifier performance characteristics are studied as the Tm dopant concentration is varied. Both single- and two-tone amplifier configurations are considered, and straight and coiled fiber cases are investigated. In all cases, the total seed power is 20 W, and, if

Optics EXPRESS

not otherwise stated, the total launched pump power is 1 kW. This total seed power was chosen to ensure that the ASE wavelengths do not grow to significant levels (<1 W). For the two-tone configuration simulations, a 10:1 seed ratio is used. The first reported metric is the fiber length that corresponds to 95% pump power absorption. The fiber performance is also characterized by the output signal power ($P_s(z = L)$), the output signal amplification efficiency ($\eta_s(z = L)$), and the peak change in temperature ($\delta T_{max} = \max\left(T(x, y, z, t)\right) - T_{ambient}$) experienced throughout the amplifier. In this study, the normalized power is obtained by dividing the given power by the total initial power, which is the sum of the total seed power and the launched pump power. The fiber signal amplification efficiency (η_s) at longitudinal point z_0 is expressed by the following formula:

$$\eta_s(z = z_0) = \frac{P_s(z = z_0) - P_s(z = 0)}{P_p(z = 0) - P_p(z = z_0) + P_t(z = 0) - \max\left\{P_t(z = 0), P_t(z = z_0)\right\}}.$$

The numerical modeling results of this study for the straight and bent fibers are illustrated in Fig. 6 and 7. For Fig. 6, plots (a) and (b), the first row shows the fiber length at which 95% of the launched pump power is absorbed. The second and third rows, respectively, depict the trends in the output signal powers and the output amplifier efficiencies under the same variations of the total dopant concentration. Figure 7 plots the peak change in temperature variations over the entire length of the straight fiber in the core (a) and polymer jacket (b) regions. The coiled fiber results are very similar to the straight fiber results, and therefore were not worth illustrating in a separate figure.

Recall that this study uses a fixed seed ratio, and thus is not optimizing the output signal power. Therefore, a color-code is implemented to better describe the amplifier output behavior. In Fig. 6, plots (a) and (b), the second and third rows of the two-tone column uses black to signify that output tone power is less than 1% of the output signal power, whereas green indicates this ratio is within 0.01 and 0.1, blue represents that it is between 0.1 and 0.5, yellow is for 0.5 to 1, and, finally, red indicates that the ratio is above 1.

The main trade-off to be considered is that a higher dopant concentration allows for a shorter fiber, which typically acts as an optical nonlinearity suppression mechanism (e.g., SBS mitigation); however, it also results in higher fiber temperatures. As described previously, higher temperatures can lead to polymer degradation or failure. The higher temperatures reduce the mode-bend-losses (review Fig. 5), including the differential mode-losses, which would make higher-order mode filtration less efficacious [25]. Near single-mode operation leads to better output beam quality. Longer fiber amplifiers are better for achieving this mode filtration effect since the losses are a scattering process as the light propagates. However, a longer fiber will also likely result in lower amplifier efficiencies since the mode-bend-losses, intrinsic silica losses, and hydroxide contamination losses will have a greater impact on the performance. Note that the heating due to absorption from the loss mechanisms is non-negligible in terms of total energy deposited throughout the fiber, and thus are included in the heat source term (Q), but they do not have a significant impact on the peak change in temperatures. Though, none of these results are surprising, or unexpected, Fig. 6 and 7 allow other researchers to approximately quantify amplifier performance, and to optimize for their given application.

3.4. Onset of ASE based on seed conditions

Amplified spontaneous emission is an issue when lasing in the 2.1-2.2 μm wavelength regime especially when one cannot achieve high enough seed powers to sufficiently saturate the active gain mechanism such that stimulated emission dominates, and suppresses the spontaneous emission. In these simulations, we are launching 1 kW of pump power into the coiled fiber, and are using a total dopant concentration of $3 \cdot 10^{26}$ ions/m^3 ($\mathcal{N}_{factor} = 1$). Note that the circular

Optics EXPRESS

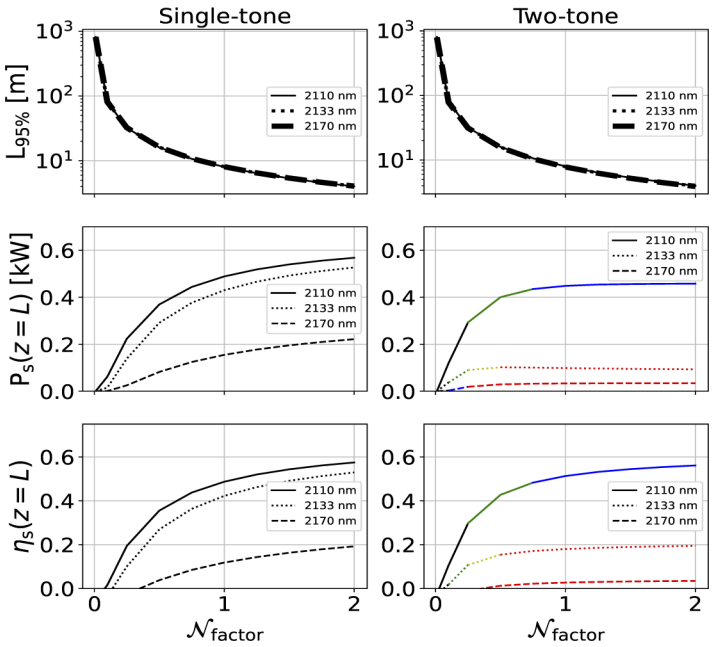

(a) Straight amplifier performances. The color-codes indicate a range of ratios of output tone power to output signal power: — <0.01, — 0.01-0.1, — 0.1-0.5, — 0.5-1.0, and — >1.0.

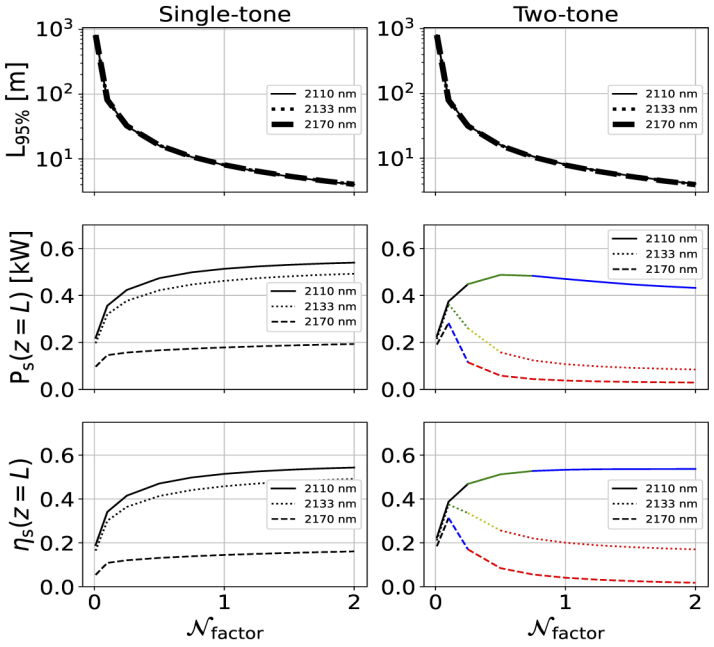

(b) Coiled amplifier performances. The color-codes indicate a range of ratios of output tone power to output signal power: — <0.01, — 0.01-0.1, — 0.1-0.5, — 0.5-1.0, and — >1.0.

Fig. 6. Straight (a) and coiled (b) amplifier lengths corresponding to 95% pump absorption, output signal powers, and output signal amplification efficiencies as the dopant concentration varies.

Optics EXPRESS

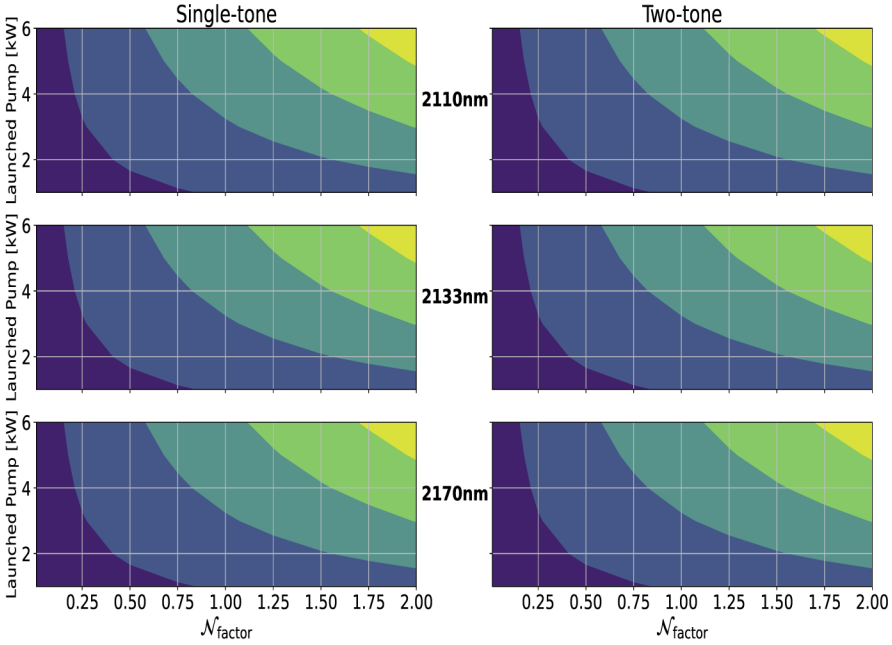

(a) Color bands relate to peak change in temperature ranges (core region) as follows:
17°C-77°C, 77°C-177°C, 177°C-277°C, 277°C-377°C, and 377°C-427°C.

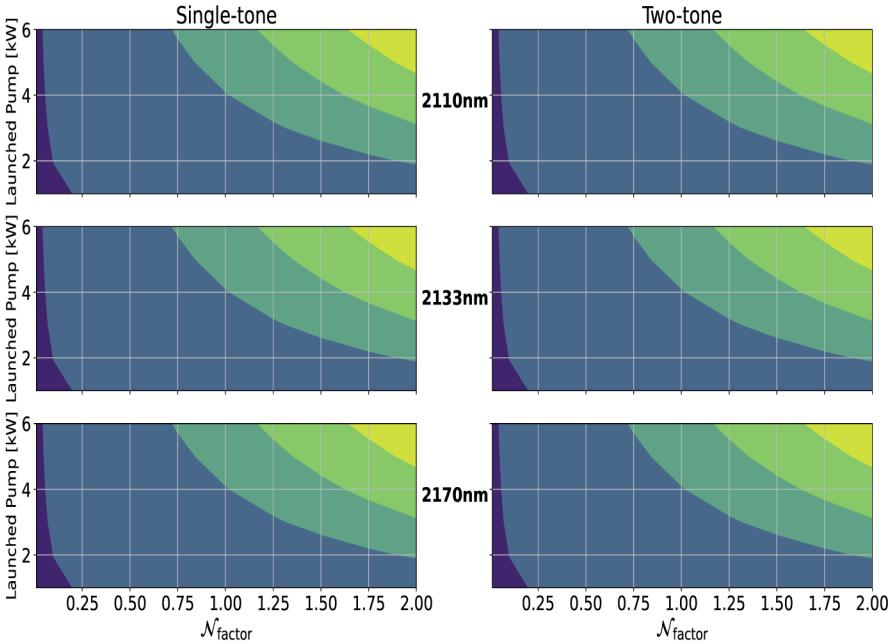

(b) Color bands relate to peak change in temperature ranges (polymer region) as follows:
17°C-27°C, 27°C-47°C, 47°C-57°C, 57°C-67°C, and 67°C-77°C.

Fig. 7. Peak change in temperature throughout the core (a) and polymer coating (b) regions as a function of launched pump power and dopant concentration.

Optics EXPRESS

bending of the fiber has little effect on the onset of ASE. Furthermore, the total ASE power is calculated by summing together the powers of each of the five ASE wavelength bins. Finally, for simplicity, we treat the fibers as being robustly single-mode, which allows us to implement the equivalent short fiber concept delineated in [13] without loss of simulation fidelity.

Figure 8 displays color contours for the maximum total ASE power levels along the amplifier based on the total seed power and the seed ratio for all three signal wavelengths. The seed ratios used for this study are 1:50, 1:25, 1:10, 1:1, 2:1, 5:1, and 10:1. These ratios are given as decimals on the abscissa of the plots. Moreover, the single-tone configured amplifier results are plotted at the seed ratio of 1:∞ = 0. For the signal wavelengths of 2133 nm and 2170 nm, review Fig. 8 plots (b) and (c) respectively, the total ASE power only increases significantly as the seed ratios approach the single-tone case, and thus are zoomed to that region. In the remaining part of these two plots, the maximum ASE power level remains below 0.01 W within the considered fiber length. Our results reflect the expectation that by increasing the total seed power, the onset of ASE is mitigated. It is also clear from the data that lower seed ratios are worse at suppressing the ASE. This is also not surprising, given that the signal is at a wavelength of low gain for the Tm dopant, and therefore needs a stronger seed to ensure stimulated emission throughout the fiber.

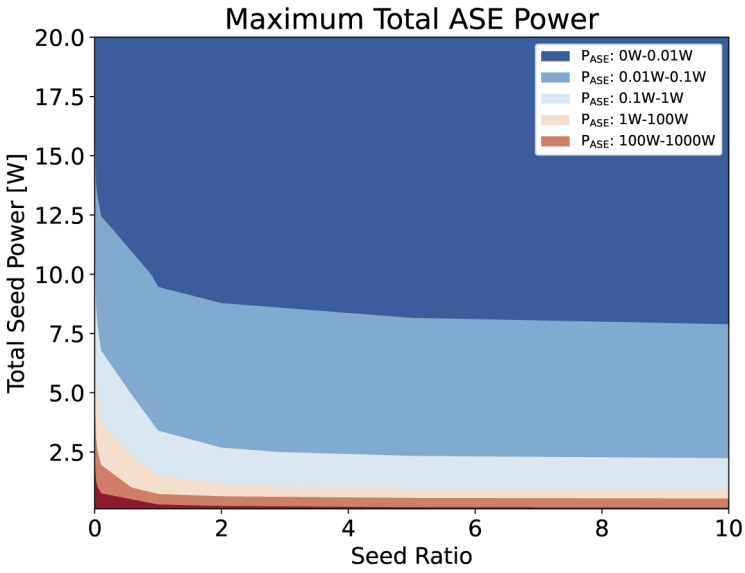

(a) λ_s = 2110 nm

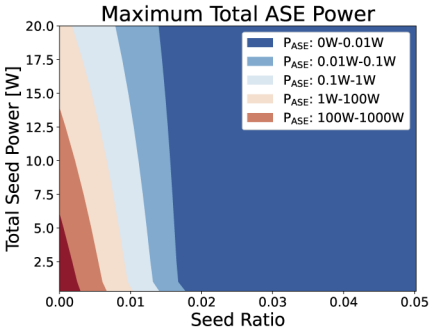

(b) λ_s = 2133 nm

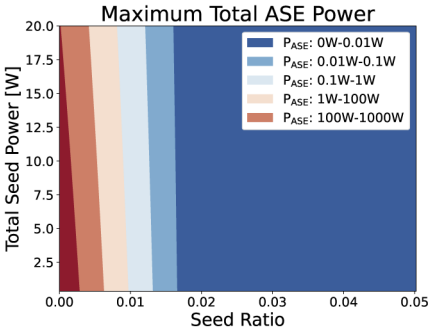

(c) λ_s = 2170 nm

Fig. 8. Maximum total ASE power levels in a straight fiber.

Optics EXPRESS

Figures 9–11 provide some examples of the ASE power profiles along the fiber length, including the sum total ASE power level, when the total seed power is 5 W. The stark difference in the ASE power levels between the two-tone (a) and single-tone (b) configurations in both Fig. 10 and 11 provide some indication as to why the ASE power levels are so low at all seed ratios for data collected at $\lambda_s = 2133$, and 2170 nm (see Fig. 8 plots (b) and (c)). In these cases, for the two-tone configuration, the tone wavelength is near the peak in the gain spectra of the Tm dopant. Thus, the tone laser saturates the gain so well that the spontaneous emission is suppressed. The signal is so weak that it does not compete well for the active gain, and the SRS effect is not strong enough to compensate. Therefore, most of the output power resides in the tone wavelength. This demonstrates that, when operating outside the main gain bandwidth, large seed ratios will likely inhibit the signal amplification. However, in the single-tone case, there is no tone wavelength to force stimulated emission, and so the ASE grows significantly.

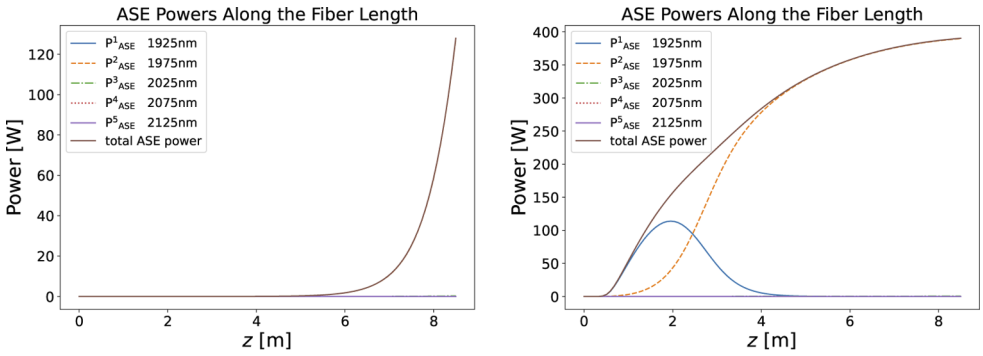

(a) Two-tone configuration with a 10:1 seed ratio.

(b) Single-tone configuration.

Fig. 9. ASE power levels when $\lambda_s = 2110$ nm using total seed power of 5 W.

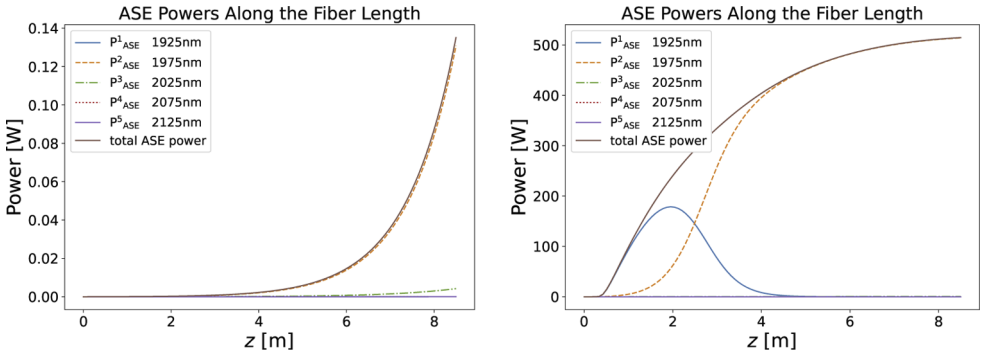

(a) Two-tone configuration with a 10:1 seed ratio.

(b) Single-tone configuration.

Fig. 10. ASE power levels when $\lambda_s = 2133$ nm using total seed power of 5 W.

3.5. *Onset of TMI*

In this subsection, we investigate the power thresholds of the TMI for both single- and two-tone amplifier configurations at $\lambda_s = 2110$ nm. The two-tone simulations are run with various seeding conditions, and include cases for two bulk Raman gain coefficients: $g_R \in \{5, 15\} \cdot 10^{-14}$ m/W. Higher Raman gain coefficients can be achieved with specific passive dopants such as germanium. Only a straight fiber is considered, and its length has been fixed at $L = 6$ m, which, in all cases, is

Optics EXPRESS

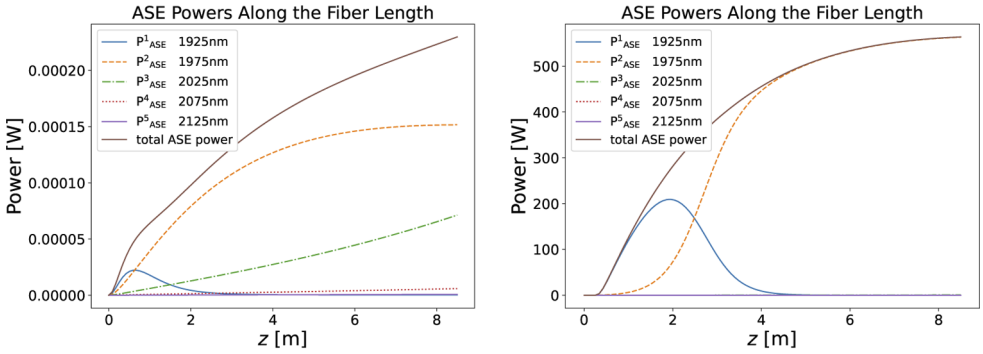

(a) Two-tone configuration with a 10:1 seed ratio.

(b) Single-tone configuration.

Fig. 11. ASE power levels when $\lambda_s = 2170$ nm using total seed power of 5 W.

sufficient to determine whether or not the amplifier has reached its TMI threshold. We consider a simulation to have reached the TMI threshold if the fundamental mode persistently transfers at least 10% of its power to higher order modes. The total seed power is set at 100 W, which ensures that the total ASE power throughout the fiber remains low (<1 W) for the single-tone case with 1 kW of launched pump power.

Table 1 lists the TMI threshold in terms of launched pump power ($P_p(z = 0)$), and then provides the corresponding output signal amplification efficiencies and maximum total ASE powers. In the table, the single-tone (1:∞ = 0 seed ratio) and the 21:10 seed ratio two-tone configurations have about the same output signal powers in a cold fiber, making these set-ups very comparable to one another. Also, recall that the two-tone configuration with a 1:1 seed ratio approximately maximizes the output signal power for the amplifier. These cases show the trend as the tone seed power is increased compared to the signal seed power.

Table 1. Launched pump power TMI threshold interval, with its corresponding output signal amplification efficiencies and maximum total ASE power range, for a straight Tm-doped amplifier with a 2110 nm signal wavelength, and a 100 W total seed power.

$g_R = 5 \cdot 10^{-14}$ $\frac{m}{W}$	TMI Power Threshold Interval [kW]	Output Signal Efficiency Interval	Maximum Total ASE Power [W]
single-tone	2.3-2.4	0.555-0.563	<1
two-tone (1:1)	1.6-1.7	0.595-0.611	20-25
two-tone (21:10)	1.9-2.0	0.575-0.595	60-75
$g_R = 1.5 \cdot 10^{-13}$ $\frac{m}{W}$	Threshold Interval [kW]	Efficiency Interval	ASE Power [W]
single-tone	2.3-2.4	0.555-0.563	<1
two-tone (1:1)	2.2-2.3	0.610-0.613	<1
two-tone (21:10)	3.0-3.1	0.610-0.625	<1

Other results of this study include the plot in Fig. 12 of the steady-state absolute temperature at the fiber's transverse center along the fiber length for both the single- and two-tone cases of the coiled fiber, using an identical launched pump power that is below their respective TMI thresholds, and that have comparable output signal powers in a cold amplifier. This plot demonstrates that the two-tone configuration does, to a small degree, spread the heat out along the fiber length a bit more than does the single-tone configuration, leading to a slightly lower peak temperature. Additionally, Figs. 13 and 14 provide visual snapshots of the output signal mode power levels

Optics EXPRESS

through time, both below and above the TMI threshold, and for both the single- and two-tone configured amplifiers.

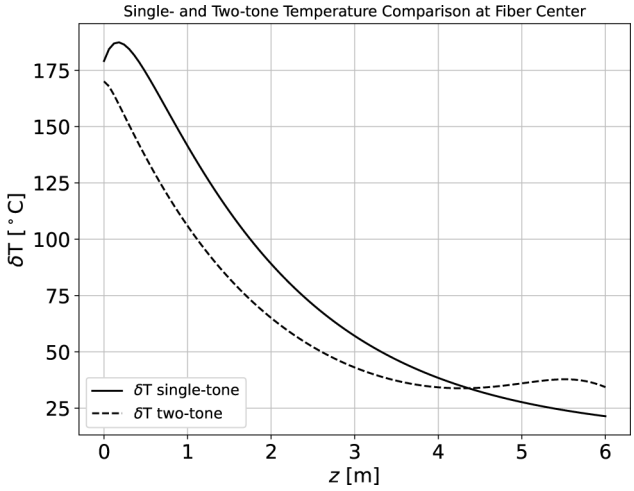

Fig. 12. Change in temperature at the fiber center comparison between single- and two-tone coiled fiber at 2110 nm after 0.01 seconds.

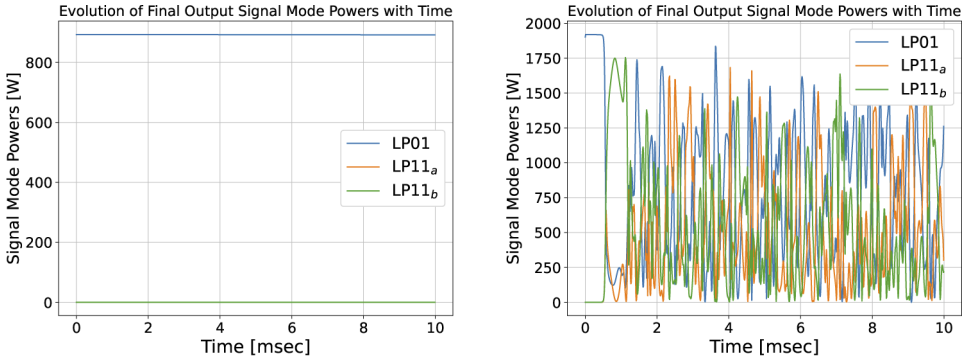

(a) Below TMI threshold.

(b) Above TMI threshold.

Fig. 13. Output signal mode powers for the single-tone configured straight amplifier operating either below (a) or above (b) the TMI threshold.

In this TMI threshold investigation, we find that the Raman gain is having a moderate impact on the TMI threshold depending on the seed ratio, and does seem to slightly mitigate the onset of the ASE. Recall that this is a large mode area fiber, and the two-tone configuration tends to reduce the onset of optical nonlinearities. The two-tone configuration, in general, is not able to significantly impact the longitudinal thermal profile compared to the single-tone configuration since the tone wavelength is relatively very close to the signal wavelength, rather than being more intermediate between the pump and signal wavelengths. Even still, our results indicate that the chosen seed ratio more prominently affects the TMI threshold and signal amplification efficiency in important ways. The two-tone configuration does seem to suppress the onset of the TMI over the single-tone configuration, at least as long as the ASE power levels are kept low. However, it is not too surprising that the TMI power thresholds are lower for the 1:1 seed ratio as compared to the 21:10 seed ratio, since the 1:1 seed ratio is closer to maximizing the output signal power. Unfortunately, the optimal seed ratio for mitigating the onset of the TMI will not

Optics EXPRESS

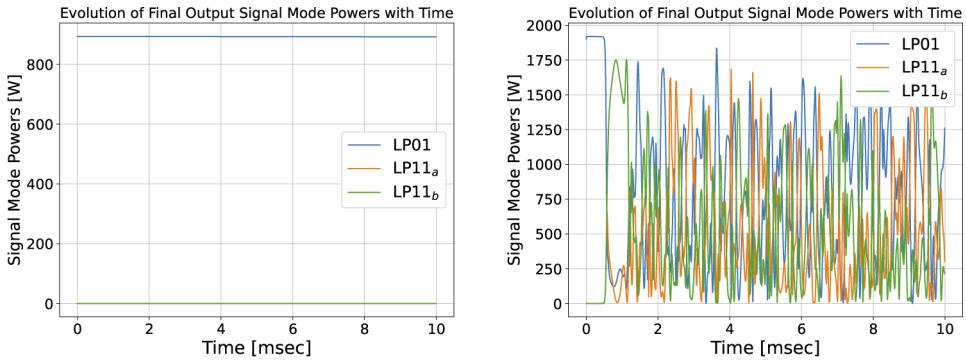

(a) Below TMI threshold.

(b) Above TMI threshold.

Fig. 14. Output signal mode powers for the two-tone configured straight amplifier (1:1 seed ratio) operating either below (a) or above (b) the TMI threshold.

likely be close to the optimal seed ratio for suppressing the onset of SBS. Even still, one may desire the lower seed ratios in order to maximize the output signal powers, and thus the signal amplification efficiency as well. And, as described previously, one problem with too high of a seed ratio is the onset of ASE; however, this is where having a larger bulk Raman gain coefficient is helpful a mitigating the onset of ASE.

4. Conclusions

This numerical simulation effort provides important quantifications of the complex performance trade-space for high-power continuous-wave Tm-doped fiber laser amplifiers operating in the 2.1-2.2 μm wavelength regime. Our studies have included the effects of changing the total dopant concentration in the amplifier, the seeding conditions (including both the total seed power and tone-to-signal seed ratios), the amplifier configuration (single- or two-tone), the magnitude of the bulk Raman gain coefficient, the coil of the fiber (straight or circularly bent), and the signal wavelength. These important amplifier characteristics include the anticipated amplifier lengths of 95% pump absorption, the guided core mode-bend-losses under different thermal loads, the signal amplification efficiencies, the signal output powers, the expected conditions for the onset of ASE and the onset of the TMI, and the predicted maximum temperatures throughout the fiber. All of these calculations are done under somewhat idealized conditions, but are indicative of what can be anticipated in real amplifiers. Our results provide relative magnitudes and trends that allow other researchers to identify potentially important parameter ranges to quantify their amplifier performance under various configurations.

Funding. Air Force Office of Scientific Research (18RDCOR018, FA9550-19-1-0237).

Acknowledgements. The authors would like to express gratitude to Dr. Brian Anderson of the Air Force Research Laboratory for his insightful comments and suggestions. Public Affairs release approval #AFRL-2020-0552.

Disclosures. The authors declare no conflicts of interest.

References

1. N. Naderi, A. Flores, B. Anderson, and I. Dajani, "Beam combinable, kilowatt, all-fiber amplifier based on phase-modulated laser gain competition," Opt. Lett. **41**(17), 3964–3967 (2016).
2. I. Dajani, C. Zeringue, T. J. Bronder, T. Shay, A. Gavrielides, and C. Robin, "A theoretical treatment of two approaches to sbs mitigation with two-tone amplification," Opt. Express **16**(18), 14233–14247 (2008).
3. C. Zeringue, I. Dajani, C. Lu, A. Lobad, and C. Vergien, "Experimental verification of two-tone amplification in single frequency fiber amplifiers," in *Nonlinear Optics: Materials, Fund. and App.*, (OSA, 2009), p. PDPA2.
4. P. Weßels, P. Adel, M. Auerbach, D. Wandt, and C. Fallnich, "Novel suppression scheme for brillouin scattering," Opt. Express **12**(19), 4443–4448 (2004).

Optics EXPRESS

5. F. Möller, V. Distler, T. Schreiber, R. Eberhardt, and A. Tünnermann, "Manipulating the heat load distribution by laser gain competition in tmi-limited fiber amplifiers," in *Fiber Lasers XVII: Technology and Systems*, vol. 11260 (International Society for Optics and Photonics, 2020), p. 1126019.
6. B. Anderson, A. Flores, J. Grosek, and I. Dajani, "High power tm-doped all-fiber amplifier at 2130 nm," in *CLEO: Science and Innovations*, (Optical Society of America, 2017), pp. SM1L–3.
7. A. Berk, P. Conforti, R. Kennett, T. Perkins, F. Hawes, and J. Van Den Bosch, "Modtran® 6: A major upgrade of the modtran® radiative transfer code," in *2014 6th Workshop on Hyperspectral Image and Signal Processing: Evolution in Remote Sensing (WHISPERS)*, (IEEE, 2014), pp. 1–4.
8. A. Berk, P. Conforti, and F. Hawes, "An accelerated line-by-line option for modtran combining on-the-fly generation of line center absorption within 0.1 cm-1 bins and pre-computed line tails," in *Algorithms and Technologies for Multispectral, Hyperspectral, and Ultraspectral Imagery XXI*, vol. 9472 (International Society for Optics and Photonics, 2015), p. 947217.
9. S. S. Inc., "Modtran® web app," http://modtran.spectral.com/modtran_home (2020).
10. B. M. Walsh and N. P. Barnes, "Comparison of tm: Zblan and tm: silica fiber lasers; spectroscopy and tunable pulsed laser operation around 1.9 μm," Appl. Phys. B **78**(3-4), 325–333 (2004).
11. J. Grosek, S. Naderi, B. Oliker, R. Lane, I. Dajani, and T. Madden, "Laser simulation at the air force research laboratory," in *XXI International Symposium on High Power Laser Systems and Applications*, (International Society for Optics and Photonics, 2017), p. 102540N.
12. T. S. McComb, "Power scaling of large mode area thulium fiber lasers in DOrchidvarious spectral and temporal regimes," Ph.D. thesis, University of Central Florida (2009).
13. J. Gopalakrishnan, T. Goswami, and J. Grosek, "Techniques for modeling fiber laser amplifiers," in *Scientific Computing in Electrical Engineering*, vol. 32 of *Mathematics in Industry* G. Nicosia and V. Romano, eds., Proceedings of The 12th International Conference on Scientific Computing in Electrical Engineering (SCEE), Taormina, Sicily, Italy (Springer, 2020), pp. 45–54.
14. S. Nagaraj, J. Grosek, S. Petrides, L. Demkowicz, and J. Mora, "A 3D DPG Maxwell Approach to Nonlinear Raman Gain in Fiber Laser Amplifiers," J. Comput. Physics: X **2**, 100002 (2019).
15. A. Smith and J. Smith, "Mode instability thresholds for Tm-doped fiber amplifiers pumped at 790 nm," Opt. Express **24**(2), 975–992 (2016).
16. S. Naderi, I. Dajani, T. Madden, and C. Robin, "Investigations of modal instabilities in fiber amplifiers through detailed numerical simulations," Opt. Express **21**(13), 16111–16129 (2013).
17. J. Gopalakrishnan, L. Grubisic, J. S. Ovall, and B. Parker, "Analysis of FEAST spectral approximations using the DPG discretization," Comput. Methods Appl. Math. **19**(2), 251–266 (2019).
18. D. Drake, J. Gopalakrishnan, T. Goswami, and J. Grosek, "Simulation of optical fiber amplifier gain using equivalent short fibers," Comput. Methods Appl. Mech. Eng. **360**, 112698 (2020).
19. R. Schermer and J. Cole, "Improved bend loss formula verified for optical fiber by simulation and experiment," IEEE J. Quantum Electron. **43**(10), 899–909 (2007).
20. O. Antipov, M. Kuznetsov, D. Alekseev, and V. Tyrtyshnyy, "Influence of a backward reflection on low-threshold mode instability in yb^3+-doped few-mode fiber amplifiers," Opt. Express **24**(13), 14871–14879 (2016).
21. V. Distler, F. Möller, M. Strecker, G. Palma-Vega, T. Walbaum, and T. Schreiber, "Transverse mode instability in a passive fiber induced by stimulated raman scattering," Opt. Express **28**(15), 22819–22828 (2020).
22. J. Schöberl, "NETGEN an advancing front 2D/3D-mesh generator based on abstract rules," Comput. & Vis. Sci. **1**(1), 41–52 (1997).
23. J. Schöberl, "C++ 11 implementation of finite elements in ngsolve," IASC, Vienna U. of Tech. (2014).
24. N. Simakov, A. Hemming, W. A. Clarkson, J. Haub, and A. Carter, "A cladding-pumped, tunable holmium doped fiber laser," Opt. Express **21**(23), 28415–28422 (2013).
25. C. Jauregui, C. Stihler, and J. Limpert, "Transverse mode instability," Adv. Opt. Photonics **12**(2), 429–484 (2020).